Production and Examination of Oxygen-Carrier Materials Based on Manganese Ores and $Ca(OH)_2$ in Chemical Looping with Oxygen Uncoupling

Nasim M. Pour
Dept. of Energy and Environment, Division of Energy Technology, Chalmers University of Technology, S-412 96 Goteborg, Sweden

Golnar Azimi and Henrik Leion
Dept. of Chemical and Biological Engineering, Division of Environmental Inorganic Chemistry, Chalmers University of Technology, S-412 96 Goteborg, Sweden

Magnus Rydén and Anders Lyngfelt
Dept. of Energy and Environment, Division of Energy Technology, Chalmers University of Technology, S-412 96 Goteborg, Sweden

DOI 10.1002/aic.14273
Published online November 9, 2013 in Wiley Online Library (wileyonlinelibrary.com)

This study concerns production of oxygen-carrier particles using six different manganese ores. The ores were made to react with $Ca(OH)_2$ at elevated temperature, forming calcium manganite. The method utilized to manufacture particles was extrusion. Methane and syngas conversion and oxygen release of the samples in inert atmosphere were investigated. The oxygen carrier based on South African (B) manganese ore, showed good methane conversion and was able to transfer oxygen corresponding to 1.5% of its mass during reduction with gaseous fuel. All examined oxygen carriers were capable of converting syngas completely. The ability to release gaseous oxygen was examined by adding wood char in a stream of nitrogen for four selected samples sintered at 1300°C/6 h. These samples released an amount of oxygen corresponding to 0.37–0.68% of their mass. The reactivity of all the ores was improved after the proposed treatments. Reactivity results of the oxygen carrier made from South African (B) ore and $Ca(OH)_2$, sintered at 1300°C for 6 h were the most promising. Attrition measurements with a jet cup of the oxygen carriers sintered at 1300°C/6 h showed that all the samples made from ores were at least three times more resistant to mechanical attrition compared to particles made from synthetic Mn_2O_3. Producing feasible oxygen carriers directly from ores could potentially cut the cost of chemical looping with oxygen uncoupling and have a significant impact on its competitiveness among other carbon capture technologies. *AIChE J*, 60: 645–656, 2014
Keywords: CO_2 capture, chemical-looping combustion, chemical looping with oxygen uncoupling, oxygen carrier, manganese ore, calcium manganate

Introduction

In recent decades, concerns about greenhouse gas (GHG) emissions and its effect on the global climate have increased significantly. Among GHGs, carbon dioxide is known to be the main anthropogenic factor for global warming. Burning fossil fuels, which constitute 80–85% of the primary energy of the world, are the main source of CO_2 emissions today. One way to mitigate CO_2 emissions from combustion of fossil fuels is carbon capture and storage (CCS). Here, CO_2 is sequestered from the flue gas produced in combustion and stored in geological formations.[1]

Correspondence concerning this article should be addressed to N. M. Pour at mnasim@chalmers.se.

Chemical-looping combustion (CLC) and chemical looping with oxygen uncoupling (CLOU)

CLC is an emerging method to capture carbon dioxide. A CLC system includes two reactors, a fuel reactor to which fuel is fed and where it reacts with the oxygen of the oxygen carriers (reaction 1), and an air reactor, in which the reduced oxygen carrier is reoxidized by air (reaction 2). The oxygen carrier normally consists of metal oxide particles.

$$\text{Fuel reactor: } (2n+m)\,\mathrm{Me}_x\mathrm{O}_y + \mathrm{C}_n\mathrm{H}_{2m} \rightarrow (2n+m)\,\mathrm{Me}_x\mathrm{O}_{y-1} + m\mathrm{H}_2\mathrm{O} + n\mathrm{CO}_2 \quad (1)$$

$$\text{Air reactor: } 2\mathrm{MexO}_{y-1} + \mathrm{O}_2 \leftrightarrow 2\mathrm{Me}_x\mathrm{O}_y \quad (2)$$

The total amount of heat released from the entire system (reaction 1 and 2) is equal to the heat released from the ordinary combustion. In CLC, the circulating oxygen carrier

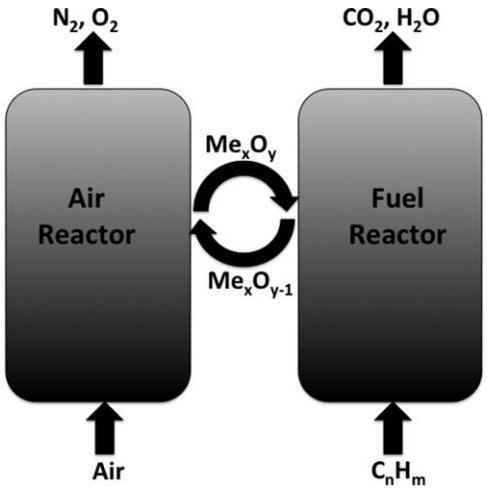

Figure 1. Schematic representation of the CLC process.

transfers oxygen from the air reactor to the fuel reactor (see Figure 1). Thereby, CO_2 and H_2O are kept separate from other flue gas components, primarily N_2 and excess O_2. Accordingly, the necessity of other gas separation units that are costly and energy consuming is eliminated.[2] Moreover, as air and fuel in CLC are added to the separate reactors, combustion takes place without flame, so NOx emission due to thermal formation of NO is naturally avoided.

For the use of solid fuels in CLC a gasification stage in which the solid fuel is gasified with steam or CO_2 is necessary.[3] This step often slows down the overall reaction rate and thereby increases the required residence time of fuel and reactor size, and thus, the overall costs. Another option is CLOU.[4] CLOU includes three steps; one in the air reactor and two in the fuel reactor. In first step in the fuel reactor, the oxygen carrier releases oxygen as gas-phase O_2 (reaction 3). In the second step, the gaseous O_2 reacts with combustible gas or char (reactions 4a and 4b). The third step is the same as in CLC where reduced oxygen carrier is oxidized with oxygen in the air reactor (reaction 5).

In fuel reactor

$$\mathrm{Me}_x\mathrm{O}_y \leftrightarrow \mathrm{Me}_x\mathrm{O}_{y-2} + \mathrm{O}_2(\mathrm{g}) \tag{3}$$

$$\mathrm{C}_n\mathrm{H}_{2m} + \left(n + \frac{m}{2}\right)\mathrm{O}_2(\mathrm{g}) \rightarrow n\mathrm{CO}_2 + m\mathrm{H}_2\mathrm{O} \tag{4a}$$

$$\mathrm{C} + \mathrm{O}_2 \rightarrow \mathrm{CO}_2 \tag{4b}$$

In air reactor

$$\mathrm{O}_2(\mathrm{g}) + \mathrm{Me}_x\mathrm{O}_{y-2} \leftrightarrow \mathrm{Me}_x\mathrm{O}_y \tag{5}$$

The net reaction of the CLOU reactions 3–5 is the same as the reaction for normal combustion or for CLC. Even though CLOU was first suggested for solid fuel application it can also be used for gaseous fuels.

Oxygen carriers

Oxides of transition metals like copper, manganese, nickel, and iron have been examined by many CLC researchers.[5–9] The selection of oxygen carriers depends on the fuel and the operational conditions of the system. High reactivity in reduction and oxidation reactions, resistance to fragmentation, attrition and agglomeration, low production cost, low environmental impacts, and high oxygen transfer capacity are some of the criteria that feasible oxygen-carrier materials should fulfill.

Manganese oxide is a good oxygen-carrier candidate due to its low price, comparably high reactivity and nontoxicity. It also shows higher oxygen transport capacity in comparison with other low-cost candidates like iron.[2] Several support materials have been investigated to improve the reactivity and mechanical strength of pure manganese oxides. Johansson et al.[10] investigated ZrO_2 as support for Mn_3O_4. Manganese-based oxygen carriers have been considered for CLOU applications as well. For instance, the CLOU effect of Fe-Mn-based oxygen carriers with gaseous and solid fuel in a small fluidized-bed batch reactor was tested by Azimi et al.[11,12] Shulman et al.[13] examined manganese oxides with MgO and optional addition of TiO_2 or $Ca(OH)_2$. Adding $Ca(OH)_2$ to manganese oxide leads to formation of perovskite phases of Ca—Mn—O ($CaMnO_{3-\delta}$). $CaMnO_{3-\delta}$ is known to have high oxygen capacity and usually maintains its perovskite structure even at highly oxygen-deficient conditions.[14,15] This could give good CLOU properties. Rydén et al.[16] examined the CLOU effect of the perovskite $CaMn_{0.875}Ti_{0.125}O_3$, which showed decent release of gas-phase oxygen. Recent experiments on $CaMn_{0.9}Mg_{0.1}O_{3-\delta}$ in Chalmers 10 kWth continuously operating reactor have shown very promising results in terms of natural gas conversion and mechanical stability.[17]

There are few studies with actual operation experiences with manganese ores, but data available indicate large loss of material by attrition,[18] whereas operation with calcium manganite shows very low loss of fines.[17]

In recent years, the possibility of using manganese ores as oxygen carriers has been examined. Although manganese ore contains impurities that can affect its physical and chemical behavior during redox cycles, it is much cheaper than pure, synthetic manganese oxides and in some cases has shown promising results.[19]

Cost of production and cost of raw materials are the two main factors in the total oxygen-carrier cost. This article examines whether it is possible to successfully manufacture feasible oxygen-carrier particles using a very cheap raw material, that is, manganese ore. The price of ores, metals, and oxides change considerably between the years, thus manganese ore cost has varied between 100 and 800 €/ton in 10 years[20] and an example of a recent index price is 5.15 $/dmtu which corresponds to 180 €/ton,[21] whereas industrial grade manganese oxide (≈99% purity) could cost, for example, 1500 €/ton. Raw materials with higher purity are even more expensive. Costs for material production are uncertain but are likely within the range 500–5000 €/ton, that is, excluding raw materials. As an example, there are spray-dried materials being sold for around 1000 €/ton. Thus, it is clear that the use of low-cost raw materials potentially could reduce the over-all cost of a manufactured oxygen carrier quite significantly. The effect of oxygen-carrier cost on the CO_2 capture cost is given by Eq. 6.

$$\mathrm{CCC}_{\mathrm{OC}} = \frac{\mathrm{C}_{\mathrm{OC}}.\mathrm{SI}}{\mathrm{SE}.\tau} \tag{6}$$

Where CCC_{OC} is the cost of CO_2 capture caused by the oxygen carrier in €/ton CO_2 captured, C_{OC} is the cost of oxygen carrier in €/ton, SI is the solids inventory in ton/MWth, SE is the specific emission in ton CO_2/MWhth, and τ is the average lifetime of the oxygen carrier. In Table 1, two

Table 1. Examples of CO_2 Capture Costs Related to Oxygen Carrier Materials

	Gas	Coal
SE, ton/MWth	0.2	0.334
SI, ton/MWhth	1	1
τ, h	5000	300
C_{OC}, €/ton oxygen carrier	1000	1000
CCC_{OC}, €/ton CO_2	1	10

examples of the effect of costs of oxygen carriers on CO_2 capture costs are given to illustrate the relation between material cost and CO_2 capture cost. The numbers for specific emissions are simply given by the heating value and the carbon content of the fuel. The solids inventory used corresponds to what is expected to be needed to attain high conversion, based on typical reactivity of oxygen carriers as well as experimental experiences in pilot operation. The estimated lifetime of oxygen carrier in gas is based on estimated lifetimes from pilot operation, for example, Källén et al.[17] For solid fuels, the lifetime is assumed to be much shorter based on the higher losses due to fuel ash. Finally, for the oxygen-carrier cost, it is assumed that a low-cost manganese ore in combination with even less costly lime [$Ca(OH)_2$] are produced at a fairly low cost. Thus, for natural gas where a long lifetime is expected the effect of material cost on the CO_2 capture cost is likely to be low. For coal on the other hand, it is more uncertain whether manufactured materials would be suitable. At present, there are no safe estimations with respect to possible lifetime of oxygen carriers with solid fuels. But with a low cost of particle manufacture and a lifetime of several hundred hours, manufactured materials could be a possibility also for coal.

Most of the research on oxygen carriers so far has been dedicated to manufactured materials using pure raw materials. Lately, very promising results have been obtained with calcium manganite materials and the purpose of this article is to see whether oxygen-carrier material costs can be reduced by the use of low-cost raw materials. The potential advantage of manganese ores with calcium added, as compared to the original ores, would be much improved performance as well as much longer lifetime.

Oxygen-carrier manufacturing methods

The method of material preparation has significant impact on the oxygen carrier properties. Shapes of particles, distribution of active metal oxide on the support material, reactivity, and mechanical strength during redox cycles are some of the parameters that are influenced by the preparation method. Another important factor is the cost of manufacturing that can be a significant share of the cost of the process.[2] Particle manufacturing normally includes three major steps.

1. Mixing and homogenization; to homogenize the mixture, several methods are utilized. In some methods, including milling and rotary evaporation, powders of metal oxide and support materials are mixed mechanically. In other mixing techniques like precipitation, dissolution, sol-gel, and solution combustion, the raw materials are mixed in a aqueous solution.[22]
2. Formation of particles; in this step, particles are formed by dispersing the well-homogenized slurry into hot air/nitrogen (Spray drying and Spin-flash drying) or into liquid nitrogen (freeze granulation), or by extruding the homogenized dough of materials in a cylinder syringe (extrusion). Impregnation is another method in which mixing and formation of particles somehow occur simultaneously. Impregnation typically involves distribution of active material on the surface of highly porous particles.[6,7,22,23]
3. Calcination of particles; to harden the particles and ensure their chemical stability and formation of the desired phases, they are calcined at high temperature. This is done in the same way regardless of the previous steps.

Scope

The aim of this work is to show that it is feasible to manufacture highly reactive oxygen-carrier particles of $CaMnO_{3-\delta}$ perovskite structure from cheap raw materials such as manganese ores and calcium hydroxide for CLOU applications. The materials were prepared by a simple extrusion method. In addition to the ability to release gas-phase O_2, reactivity with methane, syngas and wood char in CLC and CLOU applications, mechanical stability of the resulting particles were investigated.

Experimental

Oxygen-carrier manufacturing method

The oxygen carriers were prepared by a simple extrusion method. Manganese ore and $Ca(OH)_2$ were mixed mechanically. All ores contain some iron and it is very likely that iron substitutes for manganese in reacting with $Ca(OH)_2$. To assure formation of the perovskite phase of $CaMnO_{3-\delta}$, a stoichiometric amount of $Ca(OH)_2$ was, therefore, added relative to the sum of Mn + Fe in the ore. Distilled water was added to the mixture of Mn-ore and $Ca(OH)_2$ powders (particle size <90 and 46 μm, respectively). To mix the ingredients thoroughly, wet ball milling was applied. Thus, the wet mixture was stirred in an alumina jar with small stainless steel balls for 2 h. The wet homogenized slurry was put into an oven set to 200°C to be dried overnight. To get the best result in terms of viscosity, particle size and particle distribution, polyvinyl alcohol (Alfa–Aesar, average molecular weight of 25,000) as binder agent, soluble starch [$(C_6H_{10}O_5)_n$, Merck] as an auxiliary binder, LAROSTAT 519 (quaternary ammonium compound) as dispersant, ammonium hydroxide as peptizing agent and distilled water as solvent were added to the dried mixture. The well-mixed dough was extruded using a hand-held single-screw manual extruder. The extrudates were collected on a stainless steel plate and put into an oven set to 200°C to be dried overnight. A more elaborate version of this method, using rotary evaporator to homogenize the mixture, has been used before to manufacture ceria-supported oxygen carriers.[24]

To find the particles with best reactivity several samples from each Mn-ore were made and calcinated at different temperature/duration. Detailed information about different samples is presented in Table 2. The designation of the samples follows a general pattern, in which three or four letters represent an abbreviation of the Mn-ore name, the following four digits show sintering temperature and the last digits present the sintering duration in hours. A reference oxygen carrier was made from synthetic manganese oxide (Mn_2O_3) and $Ca(OH)_2$, denoted as SMN.

After calcination, extrudates were crushed and sieved. Particles in the size range of 125–250 μm were collected and

Table 2. Denotation and Calcination Schemes of Manufactured Samples

Samples	ID	Calcination Temperature (°C)/ Duration (h)
$Mn_2O_3/Ca(OH)_2$	SMN13006	1300/6
	SMN12006	1200/6
Gabon Mn-ore/$Ca(OH)_2$	GBN13006	1300/6
	GBN12006	1200/6
East European Mn-ore/$Ca(OH)_2$	ESE13006	1300/6
	ESE12506	1250/6
	ESE120012	1200/12
	ESE12006	1200/6
South African(A) Mn-ore/$Ca(OH)_2$	SAFA13006	1300/6
	SAFA120012	1200/12
	SAFA12006	1200/6
South African(B) Mn-ore/$Ca(OH)_2$	SAFB13006	1300/6
	SAFB12506	1250/6
	SAFB12006	1200/6
Brazilian Mn ore/$Ca(OH)_2$	BRZ13006	1300/6
	BRZ120012	1200/12
Egyptian Mn ore/$Ca(OH)_2$	EGP13006	1300/6

used in the experiments. In this study, oxygen carriers manufactured from six different Mn-ore were examined. Each Mn-ore has its own composition and impurities, which could lead to formation of complex chemical phases. Consequently, each ore shows different physical and chemical behavior during CLC/CLOU processes. In Table 3, composition analysis of the all used manganese ores is presented.

Experimental set up

All the experiments were performed in a straight fluidized-bed reactor with a total length of 820 mm, with a quartz porous plate of 22 mm in diameter placed 370 mm from the bottom. To make sure that the quartz reactor is completely inert and does not take part in the reactions blank test using sand as the bed material were conducted. After passing 450 mL_n/min of methane at 950°C, no sign of any reaction or oxygen release were observed. Besides, direct reactions between the quartz reactor and manganese are deemed as unlikely in this system as the reactor is made from nonporous and unreactive SiO_2 (quartz) with extremely small specific surface area.

Two Pentronic CrAl/NiAl thermocouples enclosed in quartz tubes inside the reactor measured the temperature 5 mm under and 10 mm above the porous quartz plate. The temperature presented in the article is the set-point temperature, that is, the temperature at the beginning of the reduction, measured by the upper thermocouple. The bed height in the stationary condition was measured to be in the range of 20–25 mm, when it is fluidizing its height increases up to 25–30 mm. Thus, thermocouple would be in the right place to measure the bed temperature. This is proven by observing bed particles stick to the tip of the tube holding the thermocouple and by opening the oven just after the experiments was terminated.

For experiments with inert gas and gaseous fuels, a sample of 10 g of oxygen carriers with the size of 125–250 μm was placed on the porous plate. The reactor was then heated up to 900°C in a 900 mL_n/min flow of 5% O_2 in nitrogen (oxidation period). When particles were adequately oxidized they were fluidized by 600 mL_n/min of pure N_2 (inert period). The particles were exposed to consecutive cycles of oxidizing and inert periods at a temperature of 900°C. For reactivity evaluation, the particles were exposed to 450 mL_n/min of CH_4 or syngas (50/50% H_2/CO) at 950°C. The oxidation and the reduction periods were separated by 60 s of inert periods, in which N_2 is passed through the reactor. These inert periods prevent back mixing of the product gases of the CH_4 or syngas period and oxygen of the oxidation period. Details of the experimental scheme are presented in Table 4. The methane cycles were repeated until a stable reactivity was observed.

For solid fuel experiments, a sample of 10 g oxygen-carrier particles with a size of 125–250 μm was placed onto the porous plate and heated to the temperature of interest (950°C) in a flow of 1000 mL_n/min of a gas mixture consisting 5% O_2 and 95% N_2. The particles were then alternatingly exposed to this O_2/N_2 mixture and a reducing period in which 0.1 g of wood char was introduced to the bed of oxygen-carrier particles. During reducing periods, the reactor was fluidized with 900 mL_n/min of pure N_2. Further,

Table 3. Elemental Composition Analysis of Manganese Ores in wt%

	Egyptian	East European	Gabon	South African A	South African B	Brazilian
Element	EGP	ESE	GBN	SAFA	SAFB	BRZ
Si	2.13	7.07	5.19	0.84	2.63	5.84
Al	0.58	0.24	3.26	0.20	0.17	4.05
Ca	10.15	6.76	0.37	4.12	5.42	0.21
Fe	15.95	5.76	4.92	18.61	13.08	5.61
K	0.10	0.35	0.37	0.07	0.04	0.52
Mg	0.93	1.71	0.01	0.47	0.65	0.40
Mn	37.80	48.26	49.11	44.30	49.03	53.29
Na	0.41	0.32	0.05	0.06	0.04	0.04
P	0.06	0.03	0.50	0.04	0.03	0.06
Ti	0.03	0.03	0.10	0.02	0.01	0.40

Table 4. Experimental Scheme for Gaseous Fuel; ox, in, and red Represents Oxidation, Inert and Reduction, Respectively

No. of Cycles	Reducing Gas	F_{ox} (mL/min)	F_{in} (mL/min)	F_{red} (mL/min)	t_{in} (s)	t_{red} (s)	T_{ox}	T_{red}
3	Nitrogen	900	600	–	360	–	900	900
3–6	Methane	900	600	450	60	20	950	950
3	Syngas	900	600	450	60	80	950	950
3	Nitrogen	900	600	–	360	–	900	900

300 mL_n/min of inert sweep gas (N_2) was also introduced to the system at the top of the reactor together with the solid fuel throughout the reducing period to ensure that the pulverized fuel did not get stuck in the feed line. This sweep gas did not enter the hot reaction zone of the reactor. The oxidation and the reduction periods were separated by an inert period with 900 mL_n/min of pure N_2 for 60 s. The solid fuel used for these tests was Swedish wood char with 11% volatiles, 3% moisture, and 3% ash.

Superficial gas velocity during oxidation periods in the solid fuel experiments with 1000 mL_n/min air (5% O_2) at 950°C is 22 cm/s. Minimum fluidization velocity of the samples is about 0.2–0.5 cm/s. Using formula presented by Kunii and Levenspiel, terminal velocity of tested particles would be around 50 cm/s. This places the superficial velocity used in the reactor safely between the minimum and terminal fluidization velocities.[25]

All the exhaust gases from the reactor passed through an electric cooler and after condensation of H_2O, the flue gas was led to a gas analyzer (Rosemount NGA-2000), which measures the concentration of CO, CO_2, H_2, O_2, and CH_4.

From high-frequency measurements of the pressure drop, it was possible to see if the bed was fluidizing or not. Highly fluctuating pressure drop is interpreted as stable fluidization. In contrast, when the bed is defluidized, there are no fluctuations in the measured pressure drop. A schematic description of the experimental set up can be found in Figure 2.

Data evaluation

Oxygen-carrier's conversion is evaluated by using mass-based conversion, ω, which is defined as the actual mass of oxygen carrier, m, divided by the mass of oxygen carrier in the most oxidized state, m_{ox} (Eq. 7)

$$\omega = \frac{m}{m_{ox}} \tag{7}$$

When CH_4 (Eq. 8) or syngas (Eq. 9) is used as fuel, ω is calculated as a time integral using measured outgoing gas concentrations.

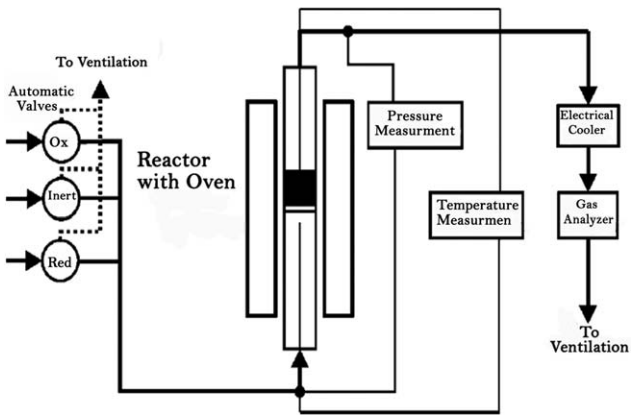

Figure 2. Schematic layout of the laboratory setup.

$$\omega_i = \omega_{i-1} - \int_{t_o}^{t_1} \frac{\dot{n}_{out} M_O}{m_{ox}} (4x_{CO_2} + 3x_{CO} - x_{H_2}) dt \tag{8}$$

$$\omega_i = \omega_{i-1} - \int_{t_o}^{t_1} \frac{\dot{n}_{out} M_O}{m_{ox}} (2x_{CO_2} + x_{CO} - x_{H_2}) dt \tag{9}$$

In the N_2 periods, ω is calculated as a time integral of outgoing O_2 concentration (Eq. 10).

$$\omega_i = \omega_{i-1} - \int_{t_o}^{t_1} \frac{2\dot{n}_{out} M_O}{m_{ox}} x_{O_2} dt \tag{10}$$

In the solid fuel experiments, the mass-based conversion during reduction with wood char is described by means of Eq. 11.

$$\begin{aligned}\omega_i = \omega_{i-1} - \int_{t_o}^{t_1} \frac{2\dot{n}_{out} M_O}{m_{ox}} \Bigg(& x_{CO_2} + 0.5x_{CO} + x_{O_2} \\ & - \left[\left(\frac{O_2}{C} \right)_{fuel} \times (x_{CO_2} + x_{CO} + x_{CH_4}) \right] \\ & - \left[\left(\frac{H_2}{C} \right) \times (x_{CO_2} + x_{CO} + x_{CH_4}) \right] - 0.5x_{H_2} - x_{CH_4} \Bigg) dt\end{aligned} \tag{11}$$

CO_2 yield (γ) is defined as the fraction of CO_2 in the outlet gas flow divided by the sum of the outgoing carbon-containing gases on dry basis (Eq. 12). By this definition a gas yield of 1 means complete conversion of the gas fuel to CO_2.

$$\gamma = \frac{x_{CO_2}}{x_{CH_4} + x_{CO_2} + x_{CO}} \tag{12}$$

In the above equations, ω_i is the mass-based conversion at a given time during a specific period i (oxidation or reduction), and ω_{i-1} is the mass-based conversion at the end of the previous period. t_0 and t_1 are the times for the start and the end of the period. x_{CO2}, x_{CO}, x_{H2}, x_{CH4}, and x_{O2} represent molar fraction of the gases CO_2, CO, H_2, CH_4, and O_2. M_O represents the molar mass of oxygen, which is 32 g/mole, and $\dot{n}_{out}$ represents the molar flow rate of the exhaust gas after condensation of H_2O. $(O_2/C)_{fuel}$, $(H_2/C)_{fuel}$ are the estimated molar ratios of oxygen and hydrogen over carbon in the fuel.

Results and Discussion

Gas conversion

Figure 3 presents the gas yield, γ, as a function of oxygen-carrier conversion, ω, during reduction with CH_4 as fuel at 950°C for the six pure, untreated ores and the five samples calcined at 1300°C/6 h.

As illustrated in Figure 3a, East European ore, ESE, which released O_2 equal to 1 wt %, showed better methane

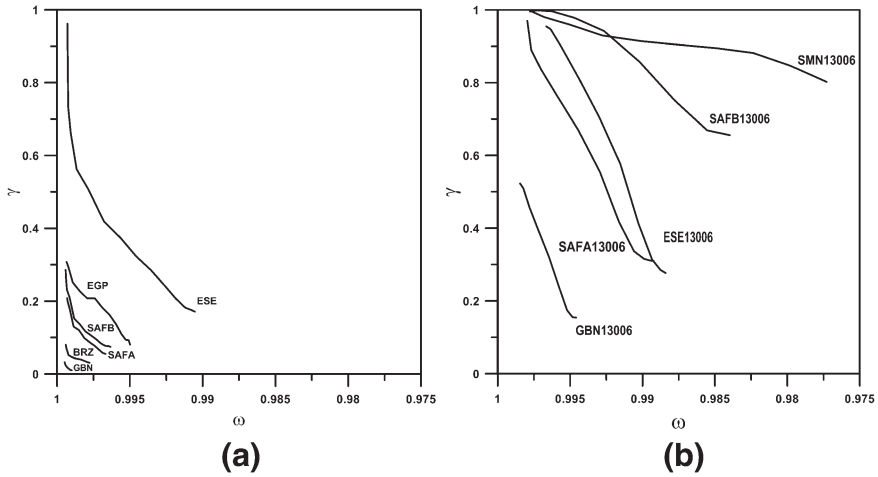

Figure 3. Gas yield as a function of oxygen-carrier conversion during reduction with CH4 as fuel at 950°C for (a) pure, untreated Mn ores and (b) the five samples calcined at 1300°C/6 h.

conversion than other ores. The sample from synthetic manganese oxide, SMN13006, had the highest conversion (with average gas yield of 90% during CH_4 period)—see Figure 3b. This is not unexpected and could be explained by the absence of impurities that results in complete formation of perovskite $CaMnO_{3-\delta}$. Among all the Mn-ore-based samples, South African (B) sample, SAFB13006, particles with 1.5 wt % oxygen release and 80% average CO_2 yield showed the highest CH_4 conversion. Conversely, Gabon manganese ore-based sample, GBN13006, with only 0.25 wt % oxygen release had the lowest CH_4 conversion. Comparing Figures 3a and b one could see that adding calcium hydroxide to the ores in all the cases enhanced their reactivity for methane conversion. The reactivity improvement was the greatest for South African ores (SAFA and SAFB). The sample based on Brazilian ore (BRZ13006) melted during calcination at 1300°C/6 h. Besides, the Egyptian ore-based sample sintered at 1300°C/6 h (EGP13006) was very soft and defluidized permanently during heat up. Thus, the corresponding graphs of these two samples are not presented in the Figure 3b.

Gas conversion versus oxygen-carrier conversion is shown in Figure 4 for samples with different sintering conditions. As seen in Figure 4a, among the oxygen carriers based on South African (B) ore, the CO_2 yield of the sample sintered at 1300°C/6 h, SAFB13006, is distinctively higher than the other samples sintered at lower temperatures. Particles of SAFB13006 could release 1.4 wt % oxygen and convert CH_4 with an average gas yield of 85%. Seemingly, for these particles increased sintering temperature improved their ability to convert methane. Conversely, as shown in Figure 4b, all South African (B) ore-based oxygen carriers show very similar reactivity in terms of syngas conversion. In fact all of them were able to convert syngas completely. The main phase of these samples was detected as $CaMn_{(1-x)}Fe_xO_3$, as will be discussed later. All the SAFBs showed stable fluidization behavior during the tests.

For the SAFAs particles, methane and syngas conversion does not seem to be influenced by changing the calcination scheme. The South African (A)-based oxygen carriers sintered at 1300°C/6 h, 1200°C/12 h, and 1200°C/6 h (SAFA13006, SAFA120012, and SAFA12006, respectively) had very similar gas conversion characteristics (see Figure 4). All the SAFA samples showed stable fluidization behavior during the experiments and the main detected phase in all the cases was $CaMn_{(1-x)}Fe_xO_3$

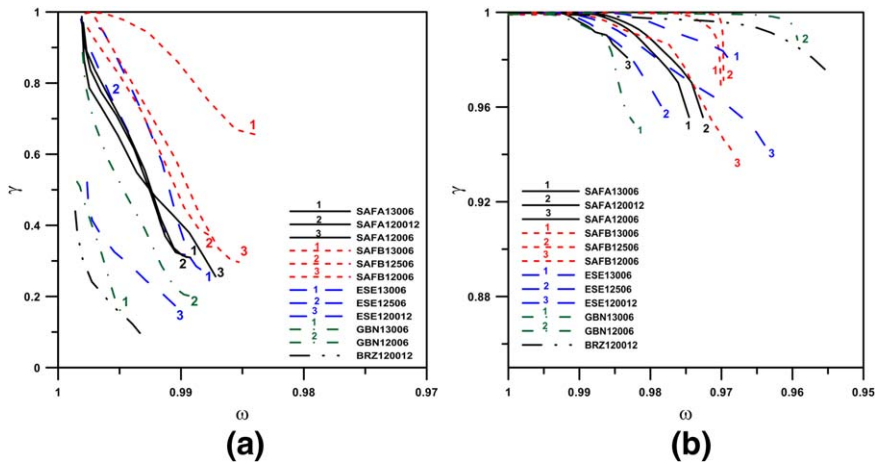

Figure 4. Gas yield as a function of oxygen-carrier mass-based conversion during reduction with (a) CH4 as fuel and (b) syngas at 950°C.

[Color figure can be viewed in the online issue, which is available at wileyonlinelibrary.com.]

As seen in Table 2, the only ore examined at all sintering schemes is the East European ore. As shown in Figure 4a, CH_4 conversion of the East European ore-based samples calcined at 1300°C/6 h and 1250°C/6 h (ESE13006 and ESE12506) with $\Delta\omega$ equal to 1% and average γ of 0.65, is almost the same. These two samples showed slightly higher reactivity than ESE120012. The ESE-samples sintered at 1200°C (ESE120012 and ESE12006) had tendency to defluidization during fuel cycles. In case of ESE12006, defluidization was so severe that no experiments with fuel could be done.

The Gabon ore-based samples, GBNs, showed the opposite behavior to increased calcination temperature; as is illustrated in Figure 4a, GBN13006, calcined at 1300°C, had a lower ability to convert CH_4 and syngas than GBN12006 (sintered at 1200°C). In fact GBN12006 could release two times as much oxygen by weight compared to GBN13006. However, both these Gabon ore-based samples have lower reactivity during CH_4 reduction compared to the other samples. Despite low methane conversion, GBN12006 shows complete syngas conversion.

By comparing the CH_4 and syngas conversion graphs of the Brazilian ore-based sample sintered at 1200°C/12 h (BRZ120012), it is seen that although this oxygen carrier had the lowest CH_4 conversion among all the tested samples, it showed complete syngas conversion.

Oxygen uncoupling behavior

For all samples, the release of oxygen in inert atmosphere by exposing oxygen carriers to N_2 was examined. Particles with high gaseous O_2 release during N_2 periods, the so-called CLOU effect, can enhance solid fuel conversion.[26]

Figure 5 presents O_2 release at 900°C as a function of oxygen-carrier mass-based conversion, ω, for the six pure, untreated manganese ores (a) and the five samples with $Ca(OH)_2$ sintered at 1300°C/6 h (b). As shown, oxygen release level in the case of all the ores goes to zero. Their capability to release gas-phase O_2 seems to be poor, with a very small $\Delta\omega$ (less than 0.1%) during the N_2 period (see Figure 5a). Conversely, samples presented in Figure 5b could release O_2 equal to 0.4 wt % during the N_2 periods.

Comparatively, the sample made from synthetic manganese oxide, SMN13006, releases O_2 at higher partial pressure ($PO_2 = 0.6\%$). In spite of having different CH_4 conversion properties, SAFA13006, SAFB13006, and ESE13006 have almost the same O_2 release level, equal to 0.4 wt % at a stable PO_2 of 0.3%. Release of oxygen from the Gabon ore-based sample, GBN13006 (with only 0.2 wt %) was lower than for the other samples.

As shown in Figure 5b, the mass-based conversion difference, $\Delta\omega$, of SAFA13006, SAFAB13006, and ESE13006 during the 360 s of N_2 period is approximately 0.4%. Conversely, $\Delta\omega$ of the different oxygen carriers in CH_4 periods is considerably higher, 0.5–2.3% (see Figure 3b). As illustrated in Figure 3, during the 20 s of CH_4 addition, $\Delta\omega = 1.5\%$ for SAFB13006, but for ESE13006, $\Delta\omega = 0.75\%$. So, all the samples lost much less oxygen during N_2 periods than in CH_4 cycles. This is partly explained by the low concentrations of oxygen that make the release slow. It is also evident from Figure 5b that most of the oxygen carriers still release O_2 after 360 s. Just as for CH_4 conversion, the samples made of Gabon Mn-ore (GBNs) shows the lowest oxygen release.

Solid fuel conversion

Solid fuel tests using wood char was conducted with the samples with the highest oxygen release during N_2 periods at 900°C, that is, SMN13006, SAFB13006, SAFA13006, and ESE13006. Figures 6a–d illustrate the outlet gas concentrations as a function of time during the reducing period with wood char at 950°C.

When the fuel is introduced to the reactor peaks of CH_4 and CO can be seen in the beginning of the reaction due to devolatilization of the fuel. Some volatiles react with the oxygen carrier and CO_2 increases rapidly. For all of the three oxygen carriers, the peak value for CO_2 is almost the same as the CO and higher than the CH_4 peak. The oxygen concentration falls to zero as the fuel conversion consumes all O_2 released. Because the fluidizing gas is nitrogen, there is no or very little gasification, so after devolatilization is finished, the remaining char can only be converted by reaction with oxygen released from the oxygen carrier. Therefore, the CO_2 is a measure of oxygen release.

Figure 7 illustrates the mass-based conversion of the four oxygen carriers with bed mass of 10 g as a function of time during the reduction with N_2 (60 s) followed by addition of

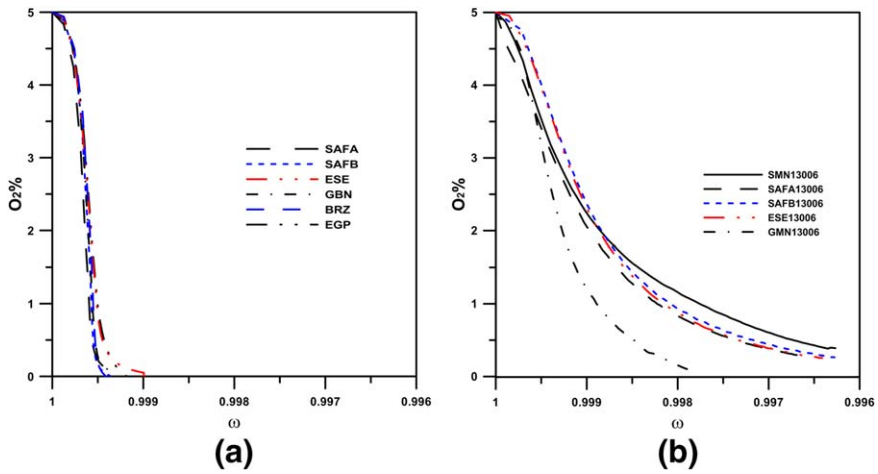

Figure 5. Oxygen release as a function of oxygen-carrier mass-based conversion during N2 period at 900°C for (a) pure, untreated Mn ores and (b) the five samples calcined at 1300°C/6 h.

[Color figure can be viewed in the online issue, which is available at wileyonlinelibrary.com.]

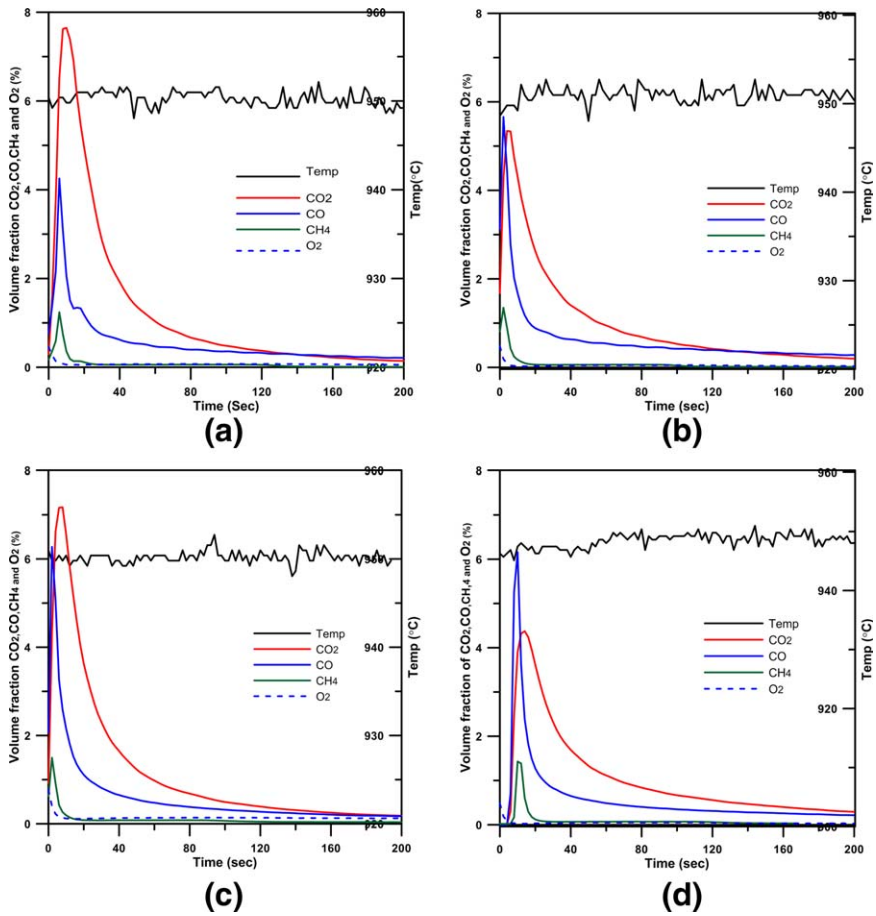

Figure 6. Concentrations for the reduction for a cycle with 0.1 g of Swedish wood char in 10 g of (a) SMN13006, (b) SAFB13006, (c) SAFA13006, and (d) ESE13006 oxygen carriers at 950°C. The fluidizing gas in reduction is pure nitrogen.

[Color figure can be viewed in the online issue, which is available at wileyonlinelibrary.com.]

0.1 g wood char at 950°C. Calculating the $\Delta\omega$ when $\omega_{t=0}$ is the mass-based conversion of particles at the end of oxidation which is assumed to be equal to 1 gives a better understanding of the ability of the oxygen carriers to release oxygen at reducing atmosphere at 950°C. In this case, $\Delta\omega$, of SMN13006, SAFA13006, SAFB13006, and ESE13006 would be 1.1, 0.68, 0.62, and 0.37%, respectively (see Figure 7). The fuel and oxidation periods in these experiments were separated by a period of N_2, so the particles release some part of their oxygen during this N_2 period prior to the fuel period. As seen, about 20 s (for SMN13006, SAFA13006, and SAFB13006) to 60 s (for ESE13006) after adding fuel the reactivity graphs become steeper. That is due to the volatiles of the fuel, which accelerate the reaction rate. When devolatilization is finished the rate of reactions decreases and the slope becomes less steep. The falling time is not significantly different between the different samples, but sometimes fuel particles stick to the tube and need to be helped to fall down into the reactor by some gentle strokes. That's why the starring time seems to differ in the figure. Important point is that during reduction with fuel, all oxygen carriers have the same general reactivity pattern, but that the different reaction kinetics differs.

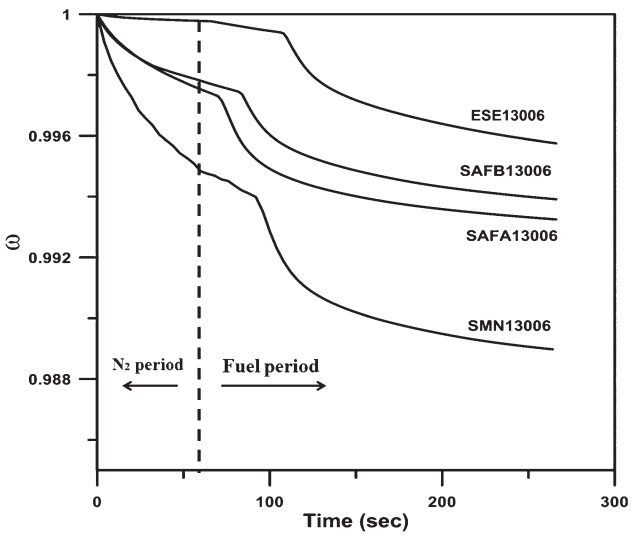

Figure 7. Oxygen-carrier mass-based conversion as a function of time during reduction with N2 followed by addition of 0.1 g wood char at 950°C.

Oxygen-carrier characterization

The phase compositions of all oxygen-carrier particles were measured using a Siemens D5000 powder x-ray diffractometer (Cu Ka1, $k = 1.54056$ Å). The x-ray diffractograms can be found in Figure 8. They do not reveal any considerable difference in phases formed for different calcination schemes

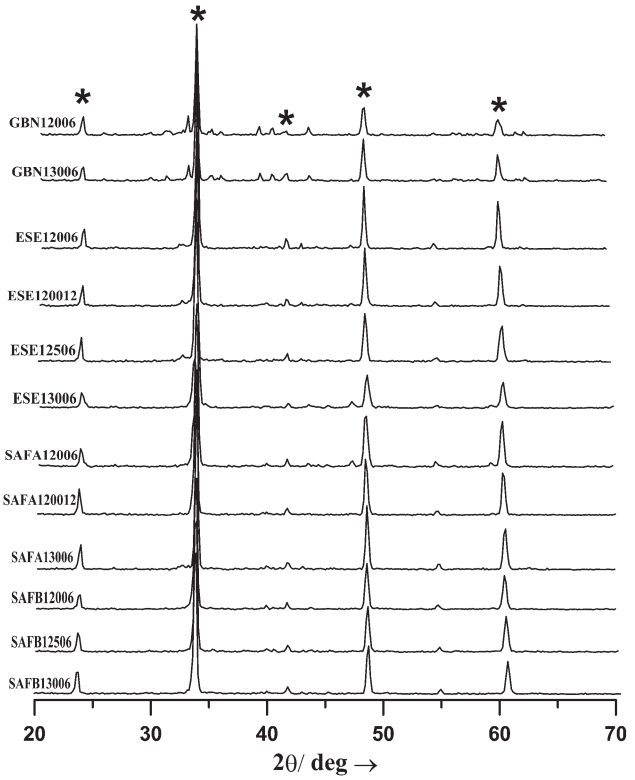

Figure 8. XRD powder patterns for the fresh samples, (*) CaMn*x*Fe(1−*x*)O3.

of the same material. Besides, the x-ray diffractograms for most of the samples were almost identical, with detection of a major phase of $CaMn_{(1-x)}Fe_xO_{3-\delta}$. Due to high iron oxide concentration in the Mn-ores, the tendency of Mn and Fe to form combined oxides and difficulties in distinguishing Fe from Mn in X-ray diffractograms (XRD), obtaining $CaMn_{(1-x)}Fe_xO_{3-\delta}$ as main phase is not surprising. In contrast, in the x-ray diffractograms of the untreated manganese ores, no $CaMn_{(1-x)}Fe_xO_{3-\delta}$ was found. Therefore, it is clear that the perovskite structure had formed after the manufacturing procedures. Moreover, XRD results for materials made from synthetic manganese oxide (SMN13006, SMN12006) showed that the desired perovskite structure of $CaMnO_{3-\delta}$ was formed in all cases. All the experimental series were ended with an oxidation phase and x-ray diffraction measurements were performed on these oxidized used samples. No significant phase change between the fresh and such used particles was seen. To summarize, it is clear that all materials formed the expected and desired perovskite structure during calcination and maintained it over the course of the experiments.

The shape and morphology of fresh and tested oxygen carriers were observed using a FEI, Quanta 200 Environmental Scanning Electron Microscope FEG. The Scanning Electron Microscopy, SEM, image of the samples looked very similar hence only SAFB13006 is presented in Figure 9. One can see that the particles have a rough structure and their surface is porous both before and after the tests. These images show that no evident changes in porosity or shape of the particles.

Table 5 presents the physical properties of the used particles. The crushing strength, that is, the force needed to fracture the particles, was examined using a Shimpo FGN-5 crushing strength apparatus. The mean value of the crushing strength for 30 particles in the range size of 180–250 μm is presented as the crushing strength value for each oxygen carrier. Measurements of the pressure drop in the reactor were used to verify that the particles fluidized properly. Several of the oxygen carriers have high crushing strength, that is, above 2 N. This is an indication that the particles could be sufficiently hard for practical applications.

As for fluidization, ESE12006 and EGP13006 defluidized permanently and caused abortion of the experiments.

The bulk density of the fresh particles in the range size of 125–250 μm was determined by measuring the mass and volume of a sample of material. The minimum fluidization velocity (u_{mf}) is calculated based on the relations by Kunii and Levenspiel.[22] The superficial velocity in the reactor system is approximately 0.17 m/s for the air reactor and 0.11 m/s for the fuel reactor with CH_4 as fuel.

The Brunauer–Emmett–Teller (BET) surface area and pore size of the particles were measured by N_2 adsorption using Micrometrics, ASAP 2020. As can be seen in Table 5, the different oxygen carriers all had similar BET surface area and pore size. It can also be seen that particles sintered at lower temperature had slightly larger surface area compared to those sintered at higher temperature. This is expected because sintering is strongly associated with pore closure.

Another important property of particles used as oxygen carriers is their resistance to physical attrition. In a fluidized bed, gas enters the bed via nozzles and often at very high velocities. Due to these gas jets, weak particles can be fragmented and/or abraded by colliding with each other and with

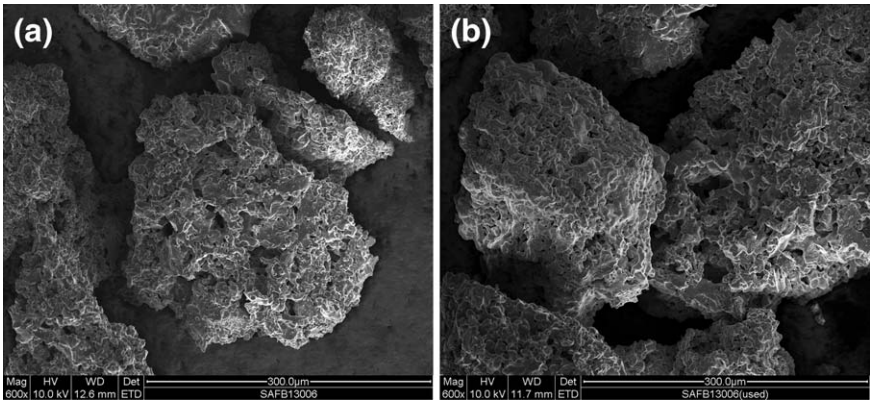

Figure 9. SEM images of SAFB13006 (a) prior to, (b) after the reactivity test. The images are 600x magnified at 300 μm range.

Table 5. Physical Properties of all the Used Samples; The Fluidization Behavior is Indicated by: 0 Not Defluidized; 1 Temporarily Defluidized or Tendencies of Defluidization; and 2 Permanently Defluidized During the Experiment

ID	Crushing Strength (N)	Fluidization Behavior	$d_{average}$ (μm)	ρ_{bulk} (kg/m^3)	u_{mf}[a] (m/s)	u_{mf}[b] (m/s)	BET Surface[c] (m^2/g)	d_{pore}[c] (nm)
SMN13006	3.0	0	152	1077	0.003	0.003	0.28	15.2
SMN12006	1.9	0	152	941	0.002	0.002	0.32	13.5
GBN13006	2.2	0	152	1496	0.004	0.004	0.14	18.4
GBN12006	1.4	1	152	863	0.002	0.002	0.37	16.5
ESE13006	2.4	0	152	1038	0.002	0.003	0.24	17.5
ESE12506	1.4	1	152	1151	0.003	0.003	0.3	12.5
ESE120012	1.2	1	152	864	0.002	0.002	0.37	15.0
ESE12006	1.3	2	152	896	0.002	0.002	0.33	9.6
SAFA13006	2.9	0	152	1937	0.005	0.005	0.3	9.3
SAFA120012	1.6	0	152	1117	0.003	0.003	0.15	16.9
SAFA12006	2.2	0	152	1022	0.002	0.003	0.21	16.0
SAFB13006	2.4	0	152	1202	0.003	0.003	0.2	11.7
SAFB12506	1.9	0	152	1065	0.003	0.003	0.2	15.0
SAFB12006	1.5	0	152	997	0.002	0.003	0.27	13.6
BRZ13006	Melted	–	152	–	–	–	–	–
BRZ120012	1.0	1	152	833	0.002	0.002	0.58	15.1
EGP13006	1.8	2	152	1188	0.003	0.003	–	–

[a]5% Oxygen (900 ml/min of Air + Nitrogen-N_2 experiments) at 950°C.
[b]CH_4 450 ml/min at 950°C.
[c]Measured by Micrometrics Tristar.

the reactor walls. Attrition resistance of selected samples was measured in a customized attrition test apparatus. The attrition test rig was designed based on the jet cup method, as described by Cocco et al.[27] The customized apparatus consists of a 39 mm high conical cup with an inner diameter of 13 mm in the bottom and 25 mm in the top. A nozzle with an inner diameter of 1.5 mm is located at the bottom of the cup, and tangentially in relation to the cup wall. During operation, air is added with a velocity of roughly 100 m/s through the inlet nozzle, creating a vortex of particles swirling upward through the cup. The cup design is intended to induce accelerated attrition with mechanisms similar to grid jets (due to the high gas velocity in the nozzle) and cyclones (due to the cone shaped particle vortex). The cup is located at the bottom of a 634 mm high gravitational particle-gas separator, basically a cone with a maximum diameter of 216 mm. Due to the increasing cross-section area, the gas velocity in the settling chamber is less than 1/20,000 compared to the inlet. The low gas velocity in the upper part of the gravitational separator allows elutriated particles to fall back into the cup, while generated fines are allowed to exit. A particle filter with a 0.01 μm filter element is located at the top of the device. The attrition test was conducted for 1 h and the filter was dismantled and weighted every 10 min. A detailed description of the apparatus and methodology can be found elsewhere (Rydén et al., submitted).

After being used in several cycles of gaseous and solid fuel experiments, samples based on South African A&B, East European and Gabon ores, in addition to sample made by synthetic Mn_2O_3, all sintered at 1300°C/6 h (SAFA13006, SAFB13006, ESE13006, GBN13006, and SMN13006) were tested in attrition test rig for 1 h. Attrition index, which basically means the mass% of the sample which was elutriated as fines from the test rig after 1 h, of five used samples was measured and the results are presented in Figure 10. As can be seen, samples made by ores have considerably lower attrition index than the one made from synthetic manganese oxide, SMN13006. As an example, particles based on the South African ore, SAFA13006, with attrition index of 3.34 mass%/h are almost 6.4 times more resistant to attrition than those made of manganese oxide, SMN13006, with attrition index of 21.3 mass%/h.

To put these numbers in some perspective, the attrition index of sample raw silica sand used as bed material for fluidized-bed combustion was 0.35 mass%/h, whereas a sample of crushed limestone for sulfur capture in fluidized bed was found to have an attrition index of 2.23 mass%/h. A sample of the commonly used oxygen-carrier material, ilmenite, which had been subjected to operation with coal, had an attrition index of 5.68 mass%/h. So from a mechanical point of view, the better of the materials examined in this study had a resistance to mechanical attrition in the same order of magnitude as limestone and ilmenite.

Discussion

Among all the Mn-ore-based samples, the South African (B) materials showed the highest CH_4 conversion, whereas, Gabon and Brazilian manganese ore-based samples showed the lowest methane conversion. The latter ores contain high wt % of Si and the highest wt % of Al. High concentration of Al could result in formation of manganese aluminate,

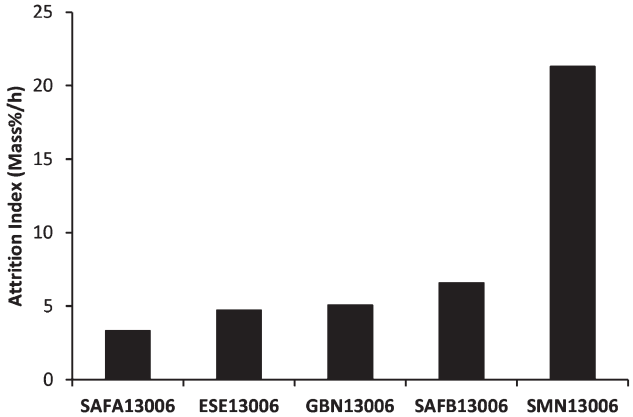

Figure 10. Attrition index of the five used samples.

which due to thermodynamic restrictions cannot be reoxidized at the operating temperature (950°C) and pressure ($PO_2 = 5\%$).[28] All the tested ores showed reactivity enhancement after the described treatments. In some cases, for example, South African ores this improvement was greater.

As shown, crushing strength and attrition index did correlate to some extent, for example, SAFA13006, ESE13006, GBN13006, and SAFB13006, the one exception being SMN13006. In general, attrition index should be a more reliable measure for the mechanical stability of the particles. Looking at the attrition and crushing strength measurement results, one can see that the mechanical stability of samples made from ores was significantly higher than that of the made from synthetic Mn_2O_3, SMN13006.

Although the oxygen loss from the material during the inert period and in the period with char conversion is explained by oxygen release, it cannot be excluded that a direct reaction occurs during the volatiles release. As seen from the methane peaks in Figure 6, the volatiles release occurs during 10 s or less after adding the fuel, and looking at the steep sections of the curves in Figure 7, it can be seen that the period of volatiles release corresponds to a $\Delta\omega$ of 0.1–0.15%. There are three possibilities;

1. the lowering of the oxygen concentration caused by the volatiles is sufficient to make the oxygen carrier release oxygen more rapidly, that is, there is no direct reaction,
2. the volatiles consume oxygen more rapidly than it can be released, and react directly with the oxygen carrier,
3. a mixture of both 1 and 2

It would, thus, be possible that part of the noted total release of 0.37–0.68% could be attributed to direct reaction, although this should be less than 0.1–0.15%. It could also be argued that even if there is some direct reaction during the period of volatiles, the material nevertheless continues to release significant amounts of oxygen after this period. This suggests that any oxygen loss during the period of volatiles caused by direct reaction could also have been released as gaseous oxygen in absence of volatiles.

Conclusions

Oxygen carriers were manufactured from six different manganese ores with addition of calcium hydroxide using an extrusion method. Conversion of CH_4 and syngas as well as O_2 release of the oxygen carriers was investigated.

Among all the tested Mn-ore-based samples, oxygen carriers made from South African-B manganese-ore sintered at 1300°C/6 h (SAFB13006) showed the best results in terms of oxygen release and CH_4 conversion. During reduction with CH_4, SAFB13006 particles could transfer oxygen corresponding to 1.5% of their mass. All the oxygen carriers were capable of converting syngas completely.

Solid fuel tests with wood char were conducted with oxygen carriers made from SMO, South African-B, South African-A, and East European manganese-ore sintered at 1300°C/6 h. These samples released an amount of oxygen corresponding to 0.37–0.68% of their mass.

Attrition resistance of the samples sintered at 1300°C/6 h was measured with a jet cup apparatus. The samples made by the ores were at least three times more resistant to attrition than particles made from synthetic Mn_2O_3. These results correlated with the crushing strength measurements to a large extent. However, crushing strength is less reliable than attrition tests for predicting material integrity in actual operation.

There was some variation in composition of the studied manganese ores, which is the likely explanation to significant differences in their properties and reactivity. This work shows that calcium manganate oxygen carriers for CLOU applications can be manufactured by low-cost ores, albeit with varying loss of reactivity compared to using the synthetic raw materials.

Acknowledgment

The research leading to these results has received funding from the European Research Council under the European Union's Seventh Framework Programme (FP7/2007–2013)/ ERC grant agreement n° 291235 and also the Swedish Energy Agency, project number 32368-1.

Literature Cited

1. Metz B, Davidson O, de Coninck H, Loos M, Meyer LA. *IPCC, 2005: IPCC Special Report on Carbon Dioxide Capture and Storage. Prepared by Working Group III of the Intergovernmental Panel on Climate Change*. Cambridge, United Kingdom and New York, NY: University Press, 2005:442.
2. Adanez J, Abad A, Garcia-Labiano F, Gayan P, de Diego LF. Progress in chemical-looping combustion and reforming technologies. *Prog Energy Combust Sci*. 2012;38(2):82–215.
3. Linderholm C, Lyngfelt A, Cuadrat A, Jerndal E. Chemical-looping combustion of solid fuels in a 10 kWth pilot-batch tests with five fuels. *Energy Procedia*. 2011;102:385–392.
4. Mattisson T, Lyngfelt A, Leion H. Chemical-looping with oxygen uncoupling for combustion of solid fuels. *Int J Greenhouse Gas Control*. 2009;3(1):9–11.
5. Dueso C, Ortiz M, Abad A. Reduction and oxidation kinetics of nickel-based oxygen-carriers for chemical-looping combustion and chemical-looping reforming. *Chem Eng*. 2012;188:142–154.
6. Cho P, Mattisson T, Lyngfelt A. Comparison of iron-, nickel-, copper- and manganese-based oxygen carriers for chemical-looping combustion. *Fuel*. 2004;83(9):1215–1225.
7. Adanez J, de Diego LF, Garcia-Labiano F, Gayan P, Abad A, Palacios JM. Selection of oxygen carriers for chemical-looping combustion. *Energy Fuels*. 2004;18(2):371–377.
8. Siriwardane R, Tian HJ, Richards G, Simonyi T, Poston J. Chemical-looping combustion of coal with metal oxide oxygen carriers. *Energy Fuels*. 2009;23(8):3885–3892.
9. Lyngfelt A. Oxygen carriers for chemical looping combustion-4000 h of operational experience. *Oil Gas Sci Technol*. 2011;66(2):161–172.
10. Johansson M, Mattisson T, Lyngfelt A. Investigation of Mn3O4 with stabilized ZrO2 for chemical-looping combustion. *Chem Eng Res Des*. 2006;84(A9):807–818.
11. Azimi G, Leion H, Mattisson T, Lyngfelt A. Chemical-looping with oxygen uncoupling using combined Mn-Fe oxides, testing in batch fluidized bed. *Energy Procedia*. 2011;4:370–377.
12. Azimi G, Rydén M, Leion H, Mattisson T, Lyngfelt A. (MnzFe1—z)yOx combined oxides as oxygen carrier for chemical-looping with oxygen uncoupling (CLOU). *AlChE J*. 2012;59(2):582–588.
13. Shulman A, Cleverstam E, Mattisson T, Lyngfelt A. Chemical-looping with oxygen uncoupling using mn/mg-based oxygen carriers—oxygen release and reactivity with methane. *Fuel*. 2011;90(3):941–950.
14. Jorge MEM, Dos Santos AC, Nunes MR. Effects of synthesis method on stoichiometry, structure and electrical conductivity of CaMnO3-δ. *Int J Inorg Mater*. 2001;3(7):915–921.
15. Bakken E, Norby T, Stolen S. Nonstoichiometry and reductive decomposition of CaMnO3-δ. *Solid State Ionics*. 2004;176:217–223.
16. Rydén M, Lyngfelt A, Mattisson T. CaMn0.875Ti0.125O3 as oxygen carrier for chemical-looping combustion with oxygen uncoupling (CLOU)—experiments in a continuously operating fluidized-bed reactor system. *Int J Greenhouse Gas Control*. 2011;5(2):356–366.
17. Källén M, Rydén M, Dueso C, Mattisson T, Lyngfelt A. CaMn0.9Mg0.1O3-δ as oxygen carrier in a gas-fired 10 kwth chemical-looping combustion unit. *Ind Eng Chem Res*. 2013;52(21):6923–6932.

18. Linderholm C, Lyngfelt A, Cuadrat A, Jerndal E. Chemical-looping combustion of solid fuels—operation in a 10 kW unit with two fuels, above-bed and in-bed fuel feed and two oxygen carriers, manganese ore and ilmenite. *Fuel*. 2012;102:808–822.
19. Leion H, Mattisson T, Lyngfelt A. Use of ores and industrial products as oxygen carriers in chemical-looping combustion. *Energy Fuels*. 2009;23:2307–2315.
20. Chuang SY, Dennis JS, Hayhurst AN, Scott SA. Development and performance of Cu-based oxygen carriers for chemical-looping combustion. *Combust Flame*. 2008;154(1–2):109–121.
21. U.S. Geological Survey. *Mineral Commodity Summaries 2011*. Reston, Virginia: U.S. Geological Survey, 2011:198 p.
22. MealBulletin.com. Mn ore index: High grade prices change direction as 38% fall further. Available at: http://www.metalbulletin.com/Article/3249806/Mn-ore-index-High-grade-prices%20changedirection-as-38-fall-further.html.
23. Lindeløv JS, Wahlberg M. Spray drying for processing of nanomaterials. International conference on safe production and use of nanomaterials. *J Phys: Conference Series* 2009;170:012027.
24. Hedayati A, Azad A-MA, Rydeń M, Leion H, Mattisson T. Evaluation of novel ceria-supported metal oxides as oxygen carriers for chemical-looping combustion. *Ind Eng Chem Res*. 2012;51:12796−12806.
25. Kunii D, Levenspiel O. *Fluidization Engineering*, 2nd ed. Boston: Butterworth-Heinemann, 1991.
26. Leion H, Mattisson T, Lyngfelt A. Using chemical-looping with oxygen uncoupling (CLOU) for combustion of six different solid fuels. *Energy Procedia*. 2009;1(1):447–453.
27. Cocco R, Arrington Y, Hays R, Findlay J, Karri SBR, Knowlton TM. Jet cup attrition testing. *Powder Technol*. 2010;200(3):224–233.
28. Mattisson T, Järdnäs A, Lyngfelt A. Reactivity of some metal oxides supported on alumina with alternating methane and oxygensapplication for chemical-looping combustion. *Energy Fuels*. 2003;17:643–651.

Manuscript received Mar. 29, 2013, and revision received Oct. 7, 2013.